


## Article

# Effect of Different Static Load Test Methods on the Performance of Combined Post-Grouted Piles: A Case Study in the Dongting Lake Area

Yu Du <sup>1</sup>, Kai Qi <sup>2</sup>, Run-Ze Zhang <sup>3</sup>, Feng Zhou <sup>2</sup> and Zhi-Hui Wan <sup>2,\*</sup> <sup>1</sup> Comprehensive Urban Management Enforcement Bureau of Yueyang City, Yueyang 414021, China<sup>2</sup> College of Transportation Engineering, Nanjing Tech University, Nanjing 211816, China<sup>3</sup> School of Civil Engineering, Southeast University, Nanjing 211189, China

\* Correspondence: wanzhahui@njtech.edu.cn

**Abstract:** To investigate the effect of combined end-and-shaft post-grouting on the vertical load-bearing performance of bridge-bored piles in the Dongting Lake area of Hunan, two post-grouted piles were subjected to bi-directional O-cell and top-down load tests before and after combined end-and-shaft grouting, based on the Wushi to Yiyang Expressway project. A comparative analysis was conducted on the bearing capacity, deformation characteristics, and load transfer behavior of the piles before and after grouting. This study also examined the conversion coefficient  $\gamma$  values of different soil layers obtained from the bi-directional O-cell test for bearing capacity calculations. Additionally, the characteristic values of the end bearing capacity, obtained from the bi-directional O-cell and top-down load tests, were compared with the values calculated using the relevant formulas in the current standards, which validated the accuracy of existing regulations and traditional loading methods. The results indicate that the stress distribution along the pile shaft differed between the two test methods. In the bi-directional O-cell test, the side resistance developed from the end to the head, while in the top-down load test, it developed from the head to the end. After combined post-grouting, the ultimate bearing capacity of the piles significantly increased, with side resistance increasing by up to 81.03% and end resistance by up to 105.66%. The conversion coefficients for the side resistance in silty sand and gravel before and after grouting are 0.86 and 0.80 and 0.81 and 0.69, respectively. The characteristic values of the end bearing capacity, as measured by the bi-directional O-cell and top-down load tests, were substantially higher than those calculated using the current highway bridge and culvert standards, showing increases of 133.63% and 86.15%, respectively. These findings suggest that the current standard formulas are overly conservative. Additionally, the measured values from the top-down load test may underestimate the actual bearing capacity of piles in engineering projects. Therefore, it is recommended that future pile foundation designs incorporate both bi-directional O-cell testing and combined post-grouting techniques to optimize design solutions.



Academic Editor: Oldrich Sucharda

Received: 17 December 2024

Revised: 2 January 2025

Accepted: 7 January 2025

Published: 9 January 2025

**Citation:** Du, Y.; Qi, K.; Zhang, R.-Z.; Zhou, F.; Wan, Z.-H. Effect of Different Static Load Test Methods on the Performance of Combined Post-Grouted Piles: A Case Study in the Dongting Lake Area. *Buildings* **2025**, *15*, 179. <https://doi.org/10.3390/buildings15020179>

**Copyright:** © 2025 by the authors. Licensee MDPI, Basel, Switzerland. This article is an open access article distributed under the terms and conditions of the Creative Commons Attribution (CC BY) license (<https://creativecommons.org/licenses/by/4.0/>).

**Keywords:** bridge engineering; combined end-and-shaft post-grouted pile; top-down load test method; bi-directional O-cell test method; conversion coefficient; bearing behavior

## 1. Introduction

Bored piles are widely used in construction projects such as high-rise buildings, large bridges, high-speed railways, and marine engineering due to their excellent bearing capacity and broad applicability [1,2]. However, the commonly used mud circulation

drilling method often results in excessively thick mud cakes on the pile surface, which reduces the side resistance of the pile shaft. Meanwhile, the accumulation of sediment at the pile bottom further weakens the end-bearing capacity. To control settlement and enhance the bearing capacity of pile foundations, traditional construction methods usually achieve this by increasing the pile diameter and length, but such approaches significantly raise construction costs. As an effective solution, the post-grouting technique has become an ideal choice for improving the bearing capacity of pile foundations due to its excellent reinforcement effect and relatively low cost [3–7]. Numerous studies [8–11] have shown that the injected grout not only improves the end-bearing performance but also enhances the interaction between end resistance and shaft resistance, thereby altering the stress characteristics of the pile shaft. This significantly affects the bearing capacity of the pile end and shaft, as well as the load transfer mechanism and overall bearing characteristics of the pile foundation. Current research on post-grouting techniques mainly focuses on single-end grouting or shaft grouting, with limited studies on the combined end-and-shaft post-grouting applications. Therefore, investigating the bearing performance of piles with combined end-and-shaft post-grouting is of significant theoretical importance and practical engineering value.

In the current engineering survey and design codes, top-down load test methods are commonly used as the primary method to determine the bearing capacity of pile foundations and to verify the reliability of pile foundation designs [12–15]. However, these methods have certain inherent limitations, as they cannot accurately reflect the ultimate bearing capacity of the soil at the pile end. This often leads to overly conservative mechanical parameters for both the pile tip and side, resulting in issues such as excessively long designs for bridge pile foundations. In particular, in water bridge engineering, traditional top-down load test methods are often limited by factors such as site conditions and loading capacity. To address these issues, many scholars have researched the bi-directional O-cell test method, providing new solutions to overcome the limitations of traditional static load tests for pile foundations [16–18]. Currently, several countries have developed relevant testing standards, and China has incorporated this technology into the national industry standard “JGJ/T 403-2017 Technical code for self-balancing static load tests on building foundation piles” [19]. The basic principle of the bi-directional O-cell test method is to set an O-cell inside the pile shaft or at the pile end. By applying pressure through the load box, upward and downward displacements are generated in the pile shaft, and the reaction force of the pile shaft is used to simulate the actual load state of the pile foundation, directly calculating the ultimate end resistance of the pile. This method has the advantage of wide applicability and can be performed at various test sites, as shown in Figure 1. Related studies have shown that the bi-directional O-cell test method can effectively improve the accuracy and reliability of pile foundation design. Dai et al. [20] and Safaqah et al. [21] conducted bi-directional O-cell tests on 14 large-diameter post-grouted piles for the Sutong Yangtze River Bridge, and the results showed that post-grouting not only enhanced pile end resistance but also improved the properties of the pile–soil interface, leading to substantial economic benefits in bridge pile foundation design. Nguyen and Fellenius [22] performed similar studies on two large-diameter post-grouted piles at the Binh Lo Bridge in Vietnam, finding that post-grouting at the pile end significantly improved the bearing capacity of the pile foundations. Zhou et al. [23] combined on-site bi-directional O-cell tests at the Guanyinsi Yangtze River Bridge in Hubei Province to study the bearing performance of distributed grouted bored piles in deep gravel layers, revealing that distributed post-grouting effectively enhances the ultimate bearing capacity and reduces pile head settlement. Wan et al. [24] conducted large-tonnage bi-directional O-cell tests on eight large-diameter rock-socketed bored piles in Shenzhen, showing that combined post-grouting

significantly improved bearing and deformation performance, with increased side and end resistance in strongly weathered rock layers. Although many studies have focused on the application of the bi-directional O-cell test method, there is still a lack of reports comparing the effects of the bi-directional O-cell test and top-down load test on the performance of post-grouted piles.

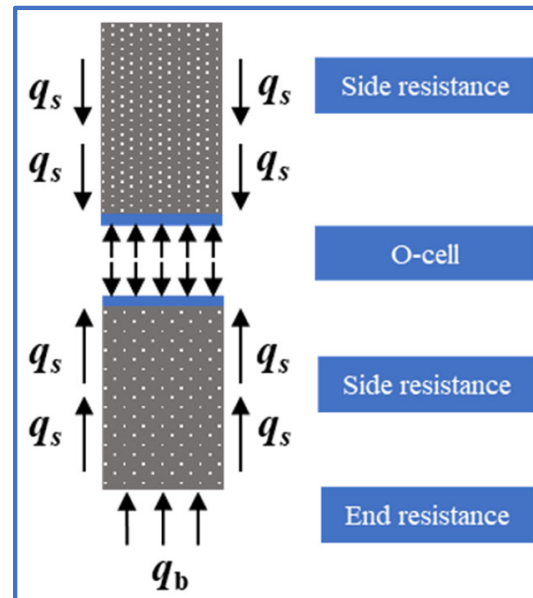


**Figure 1.** Schematic diagram of the bi-directional O-cell test.

Therefore, a comparative study of the bi-directional O-cell test method and top-down load test method, based on field tests, is of significant theoretical importance and practical value for optimizing the design of bored piles. In this context, this paper is based on the Wushi to Yiyang Expressway project located in the Dongting Lake region of Hunan Province and investigates the impact of the bi-directional O-cell test method and top-down load test method on the bearing performance of bored piles before and after combined grouting. Additionally, a comparative analysis is conducted between the bi-directional O-cell test method, the top-down load test method, and the end-bearing capacity characteristic values calculated using current code formulas. The purpose of this study is to verify the accuracy of the top-down load test method and code-based calculations to provide theoretical support and reference for the design of bridge foundations in the Dongting Lake region of Hunan Province and similar geological conditions.

## 2. Overview of Site Stratigraphy, Test Piles, and Static Load Tests

### 2.1. Site Stratigraphy and Engineering Geology

The Wushi to Yiyang Expressway project is located in the northeastern part of Hunan Province, along the southern edge of Dongting Lake, as shown in Figure 2. The terrain along the route mainly consists of hills, uplands, river terraces, and lakeside plains. Due to the terrain and geological conditions of the lake area, as well as the need for flood prevention and flood control, the project route extensively utilizes elevated bridge structures. The bridge length in the lake area exceeds 30 km. Within the scope of the site investigation, the subsurface layers primarily consist of Quaternary artificial fill, mucky soil, silty clay, sand, and gravel layers. The physical and mechanical properties of each soil layer within the length range of the test piles are presented in Table 1.

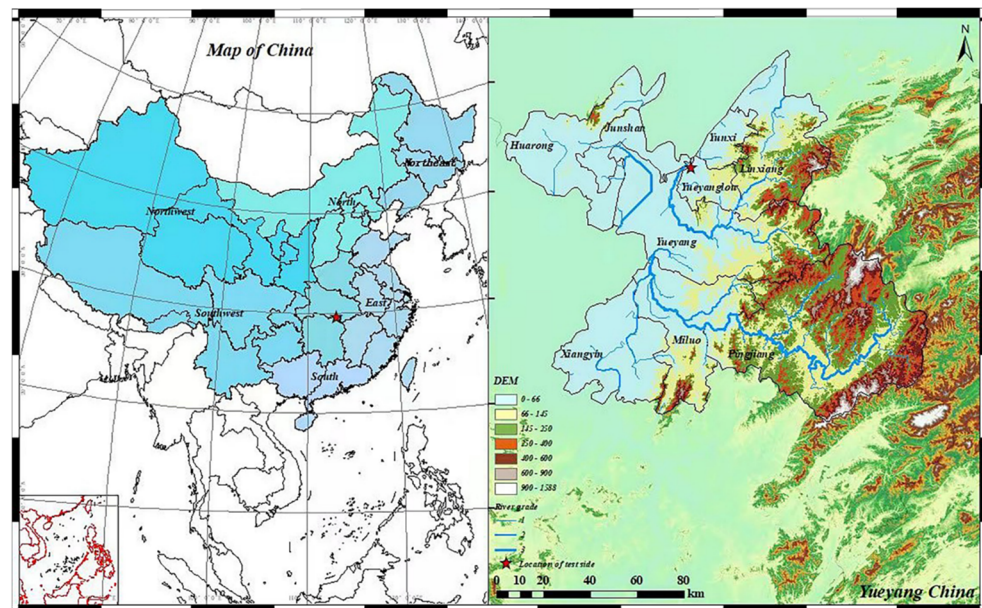


Figure 2. Location of the test site.

Table 1. Geological parameters of each soil layer at the test site.

Soil Layer No.	Soil Layer Name	$\gamma$ ( $\text{kN}\cdot\text{m}^{-3}$ )	$c$ (kPa)	$\varphi$ ( $^{\circ}$ )	$E_s$ (MPa)	$f_{a0}$ (kPa)	$q_{sik}$ (kPa)
1	Quaternary artificial fill	17.8	21.10	6.8	2.21		
2-1	Silty sand	18.77	29.27	11.5	5.72	35	50
3-2	Mucky soil	17.3	28.84	6.95	5.82	50	25
4-1	Silty clay	18.3	33.83	7.48	4.9	50	55
5-2	Coarse sand	18.45	21.58	15.9	5.67	70	175
6-2	Gravel	22.6	17.67	18.1	6.49	130	225

Note:  $\gamma$  is the natural weight of each soil layer;  $c$  and  $\varphi$  are the cohesion and internal friction angles of each soil layer derived from the drained shear test, respectively;  $E_s$  is the compressibility modulus of each soil layer;  $f_{a0}$  is the basic allowable value of the bearing capacity; and  $q_{sik}$  is the standard value of the side resistance.

## 2.2. Overview of Test Piles

The two in situ piles selected for testing in the Wushi to Yiyang Expressway project were constructed using the drilled shaft method. The elastic modulus of the piles, denoted as  $E_c$ , was presumed to be 30 GPa. The test pile labeled TP1 has a diameter of 1.2 m and a length of 23 m while the test pile labeled TP2 has a diameter of 1.6 m and a length of 30 m. Both piles are founded on a bearing layer consisting of 6-2 gravel. A combined end-and-shaft grouting technique was used for the test piles. For end grouting, the straight-pipe method was used, with three steel grouting pipes with a diameter of 30 mm and a wall thickness of 2.5 mm. For shaft grouting, the annular-pipe method was applied, using two grout annular pipes with the same diameter. The construction sequence involved performing shaft grouting first, followed by end grouting. Shaft grouting was carried out according to the “top to bottom” principle, and the time interval between shaft and end grouting was no less than 2 h. According to the relevant standards [25], the end grout mixture was prepared with P.O. 42.5 ordinary Portland cement, with a water-to-cement ratio of 0.6. The cement quantities for grouting TP1 and TP2 were 5000 kg and 7800 kg, respectively, and the grouting pressure ranged from 0.56 to 3.4 MPa. The main design parameters of the test piles are shown in Table 2. The geological profile, reinforcement layout, grouting pipe arrangement, and construction flow chart for the test piles are shown in Figure 3, Figure 4, and Figure 5, respectively.

Table 2. Main design parameters of test piles.

Test Pile No.	L (m)	D (m)	L/D	Bearing Stratum	Grouting Volume (kg)
TP1	23	1.2	19.17	Gravel	5000
TP2	30	1.6	18.75	Gravel	7800

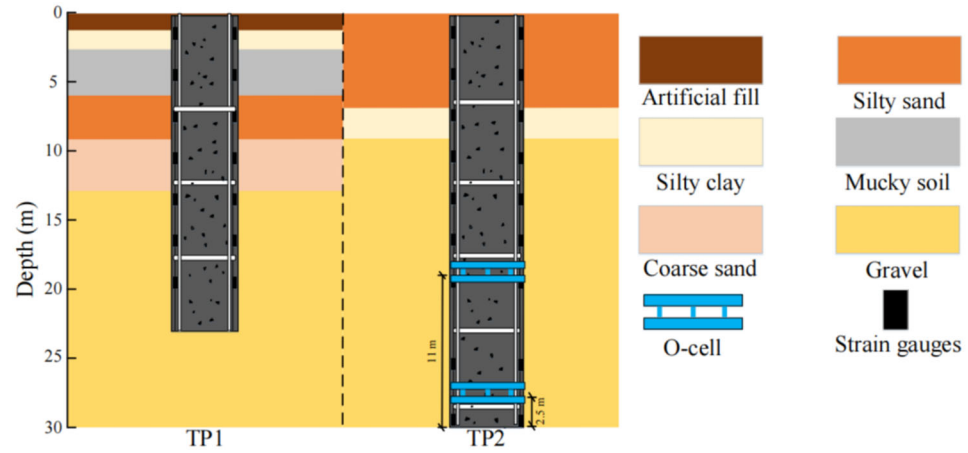


Figure 3. Soil layer distribution profile of the test piles.

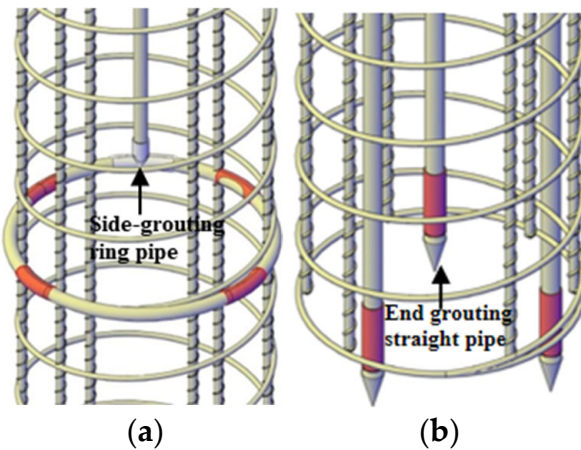


Figure 4. Grouting pipe arrangement diagram: (a) Side grouting ring pipe and (b) End grouting straight pipe.

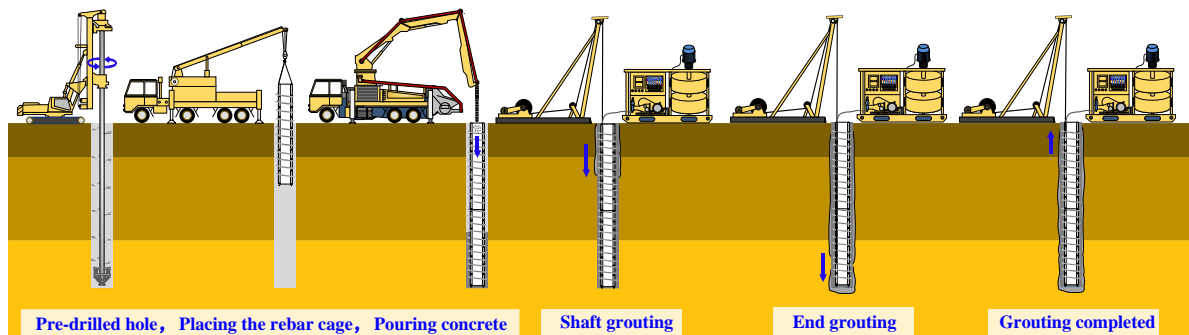


Figure 5. Construction flow chart of the combined post-grouted pile.

2.3. Static Load Test

The static load test for the test pile consists of two stages. Stage 1 refers to the static load test conducted before grouting, which is carried out to evaluate the load-bearing capacity of the pile after the concrete is poured and the pile is formed. Stage 2, on the other

hand, refers to the static load test performed after the grouting process is completed, once the cement grout has been injected and allowed to cure to achieve the design strength. Numerous practical studies [2,19,26] have shown that, after the cement grout is injected and allowed to cure for 20 days, the surrounding soil fully recovers and the strengthening reaction of the grout is nearly complete. Therefore, it can be concluded that the results of the static load test in Stage 2 are minimally influenced, or even unaffected, by the results of the Stage 1 test.

(1) Top-down load test

The test pile TP1 adopts the static load test using the heaped load method, in accordance with the requirements of the “JTG/T 3650-2020 Technical specifications for construction of highway bridges and culverts” [27]. The test employs a slow-maintenance load method, with a loading level of 900 kN. The first stage of loading is applied at twice the incremental load, i.e., 1800 kN. If the settlement rate is less than 0.1 mm per hour and this occurs twice consecutively (starting 30 min after the application of the incremental load, with settlement recorded every 30 min over a period of 1.5 h), it is considered that the settlement has stabilized, and the next load stage can be applied. The unloading process follows the guidelines specified in the standard. The static load test employs a reaction beam system, with concrete prefabricated blocks as counterweights. Four 500-ton hydraulic jacks, driven by a hydraulic electric pump system, are used for load application. Settlement measurements are taken using a static load testing device. A schematic diagram of the heaped load method test is presented in Figure 6.

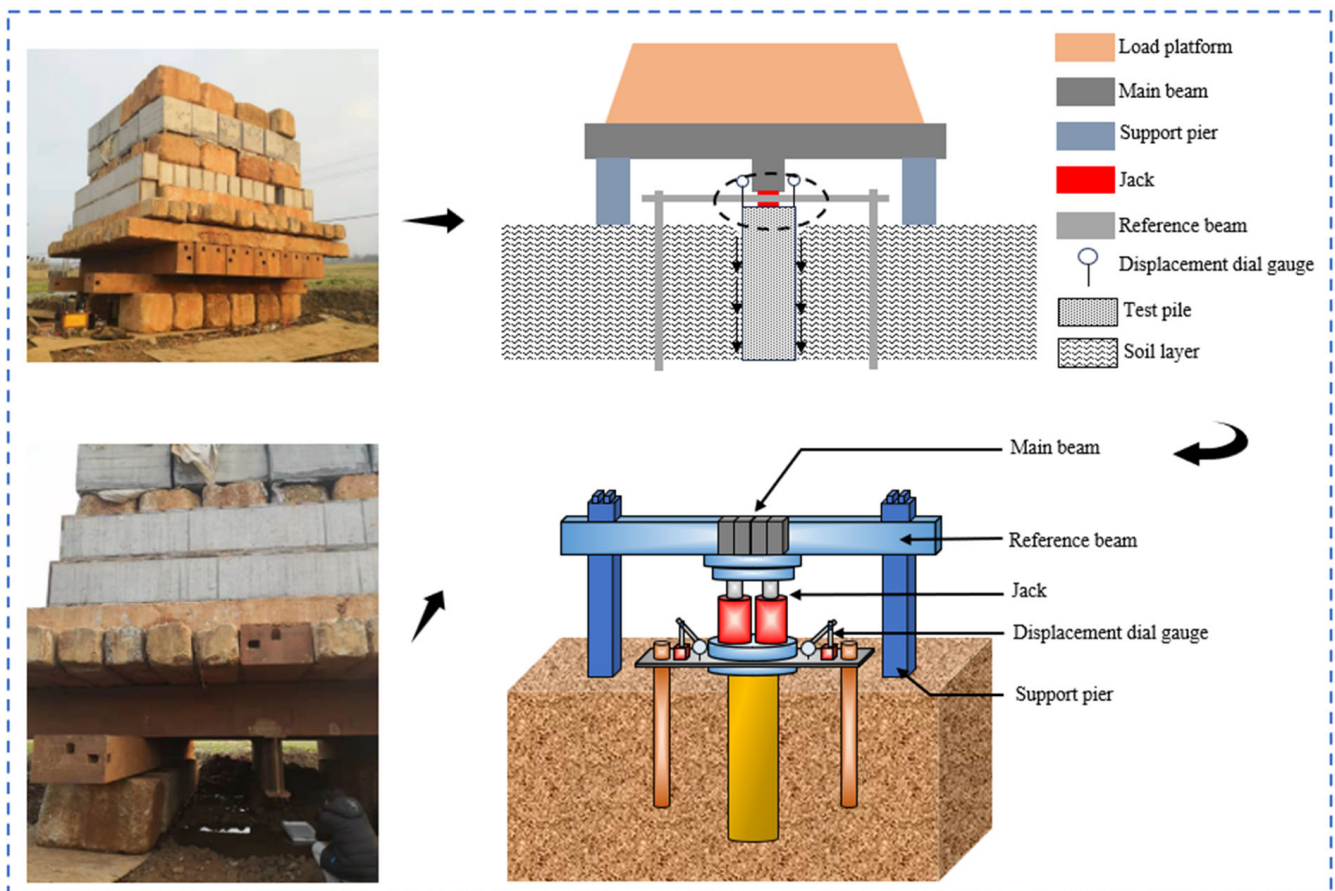
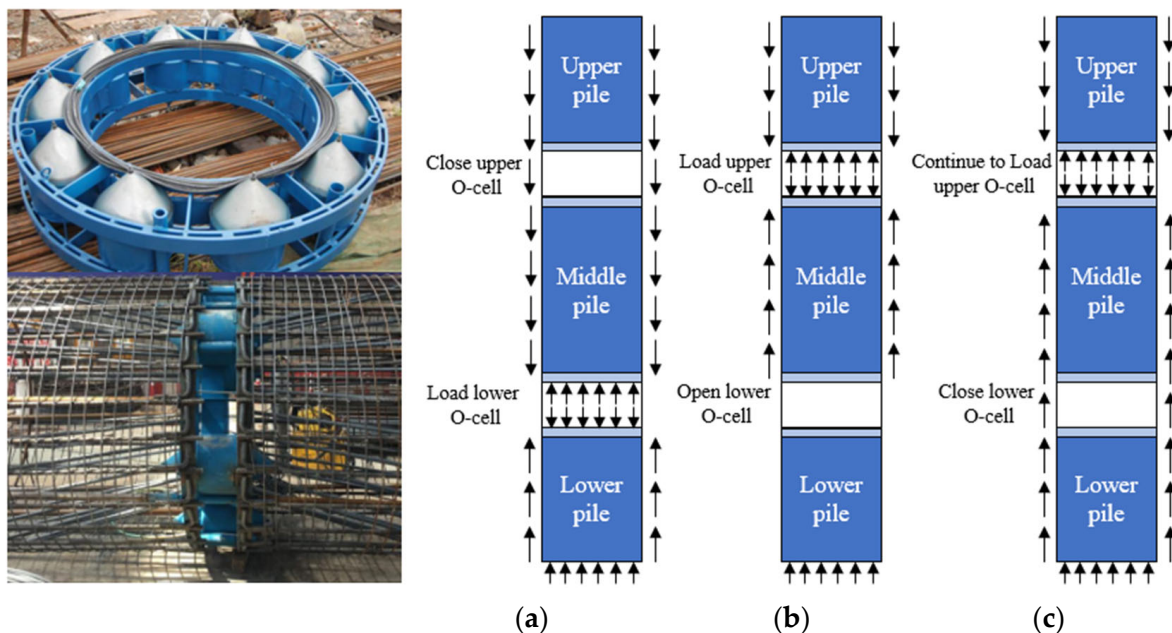


Figure 6. Diagram of the top-down load test method.

## (2) Bi-directional O-cell test

The test pile TP2 employs the bi-directional static load test method with double-level O-cells, with specific procedures following the “JGJ/T 403-2017 Technical specifications for the static loading test of the self-balanced method of building foundation piles” [19]. The test uses a slow-maintained load method, with each loading increment set at 1000 kN, and the initial loading level is twice the standard load, i.e., 2000 kN. The unloading process is conducted in stages, with each unloading step being three times the corresponding loading step. Two O-cells are embedded in the pile shaft: the upper O-cell is located 11 m from the pile tip, and the lower O-cell is positioned 2.5 m from the pile tip. Data obtained from strain gauges arranged at the interfaces between different soil layers along the pile shaft are used to calculate the axial force of the pile and indirectly estimate the side resistance in each soil layer. The end resistance is determined by subtracting the side resistance of the lower section from the value measured by the lower O-cell. During the test, four electronic displacement transducers are used to measure the displacement changes of the test pile. These displacement transducers are mounted on a reference beam using magnetic brackets, with two transducers measuring displacement at the top plate of the O-cells and the other two measuring displacement at the bottom plate of the O-cells. A schematic diagram of the double-level bidirectional O-cell test setup is shown in Figure 7.



**Figure 7.** Schematic diagram of the bi-directional O-cell test method with double-level O-cells. (a) First, load the lower O-cell. (b) Second, open the lower O-cell, then load the upper O-cell. (c) Third, close the lower O-cell, then load the upper O-cell continuously.

### 3. Static Load Test Results and Analysis of Post-Grouted Bored Piles

#### 3.1. Load–Settlement Curve

The measured  $Q$ - $s$  curves for test piles TP1 and TP2 before and after grouting are shown in Figure 8. Using the equivalent conversion method outlined in JGJ/T 403-2017 [19], the bi-directional O-cell test results for test pile TP2, both before and after grouting, were converted into corresponding pile head load–settlement ( $Q$ - $s$ ) curves typically associated with the top-down load test, as shown in Figure 9.

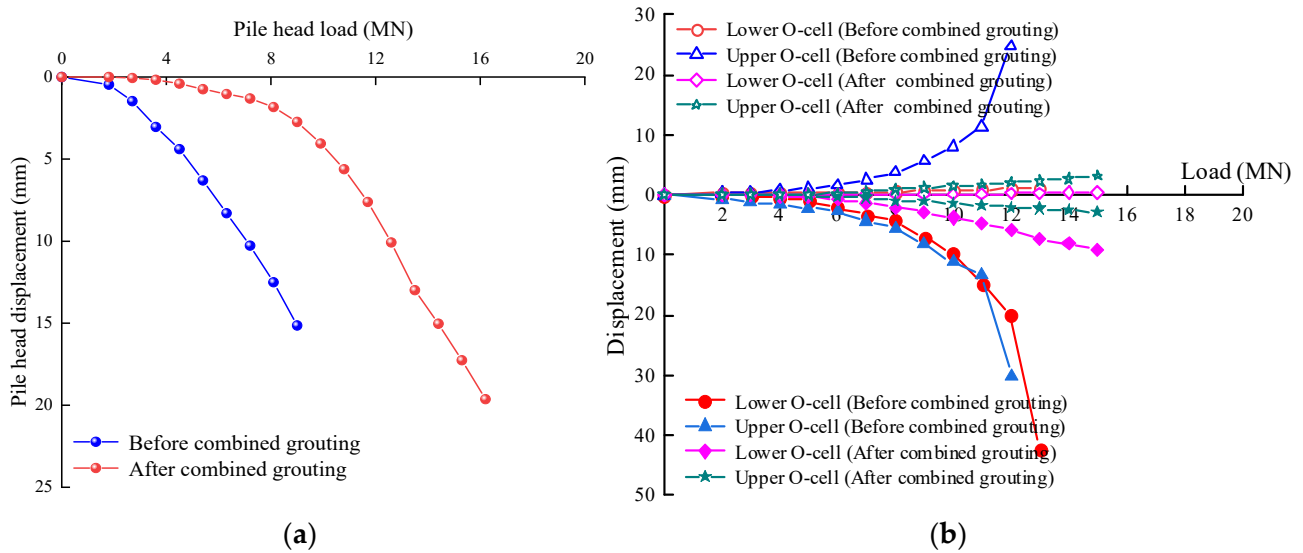


**Figure 8.**  $Q$ - $s$  curves before and after the combined grouting of the test piles: (a) TP1 and (b) TP2.

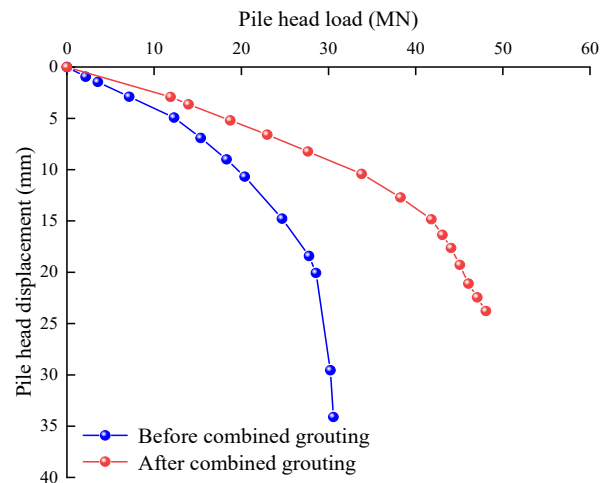


**Figure 9.** Equivalent conversion  $Q$ - $s$  curve before and after the combined grouting of TP2.

As illustrated in Figure 8, there are significant differences in the  $Q$ - $s$  curves corresponding to the two loading methods. For test pile TP1, the curve is relatively flat in the initial loading stage. As the load level increases, the side resistance becomes progressively significant, leading to an accelerated rate of displacement growth and a steeper slope of the curve. When the load at the top of the pile reaches or approaches its ultimate bearing capacity, the load–displacement curve exhibits a sharp decline. In contrast, for the test pile TP2, the load is applied via an O-cell located within the pile during the initial loading stage. The upper and lower plates of the O-cell exert loads on the respective upper and lower sections of the pile. The displacement primarily results from the elastic deformation of the pile itself, as well as the localized response of the surrounding soil. As the load level increases, relative displacement develops between the pile and the surrounding soil, which further mobilizes the side resistance. The upward and downward displacements observed in different sections of the test pile demonstrate an increasing trend, with the slope of the curve progressively steepening, ultimately resulting in a sudden variation.

Simultaneously, as illustrated in Figures 8a and 9, the  $Q$ - $s$  curves for test piles TP1 and TP2 following combined grouting are notably affected by the length-to-diameter ratio of the individual piles. The initial slope of the  $Q$ - $s$  curves for test piles TP1 and TP2 decreases with the increase in the length-to-diameter ratio of the single pile. In addition, the  $Q$ - $s$  curves of



the two test piles before grouting exhibit significant inflection points, demonstrating a trend characterized by initial gradual changes followed by a steep decline. In comparison to the  $Q$ - $s$  curves obtained prior to grouting, the curves for the test piles after grouting demonstrate a markedly shallower slope leading up to the inflection point, suggesting a considerable enhancement in bearing capacity. During the initial loading phase, the settlement of the pile tops increases in a nearly linear manner as the load on the pile tops rises. As the load continues to increase, notable differences in the bearing capacity of the test piles become increasingly apparent before and after grouting. Under identical pile top loads, the settlements of the two test piles after grouting were significantly lower than those observed before grouting, and the inflection point also shifted to a higher load level. According to JGJ 106-2014 “Technical code for testing of building foundation piles” [28], the bearing capacities of the single test piles were determined. Before grouting, the bearing capacities of test piles TP1 and TP2 were measured at 9.00 MN and 28.56 MN, respectively. After grouting, their bearing capacities increased to 16.20 MN and 48.09 MN, representing improvements of 80.00% and 68.30%, respectively. This indicates that the combined grouting technique can effectively enhance the bearing capacity of pile foundations. At the same time, the  $Q$ - $s$  curve of the pile after grouting exhibits a shallower slope in the gradual change segment when compared to the  $Q$ - $s$  curve of the pile before grouting. This indicates that the upward movement of the cement grout and its subsequent downward infiltration have improved the mud skin effect on the side of the pile, effectively controlling the pile head settlement under the action of the ultimate load.

### 3.2. Axial Force of the Pile

Strain gauges for Test Pile 1 were installed along the pile shaft at depths of 1.2 m, 2.2 m, 6.6 m, 9 m, 12.4 m, 16.7 m, 18.7 m, and 21.1 m from the mud surface. Strain gauges for Test Pile 2 were installed at depths of 3.5 m, 6.5 m, 9.4 m, 14 m, 19 m, 21.5 m, 25.5 m, 27.5 m, and 29 m from the mud surface to measure the strain of the piles. Based on the principle of coordinated deformation between the reinforcement and concrete and considering the relative axial stiffness of the reinforcement and concrete cross-section, the axial force at the pile cross-section can be calculated. Using the strain data collected from the strain gauges under different loading levels, the axial force ( $F$ ) distribution along the depth ( $h$ ) of test piles TP1 and TP2 was derived and plotted, as shown in Figure 10.

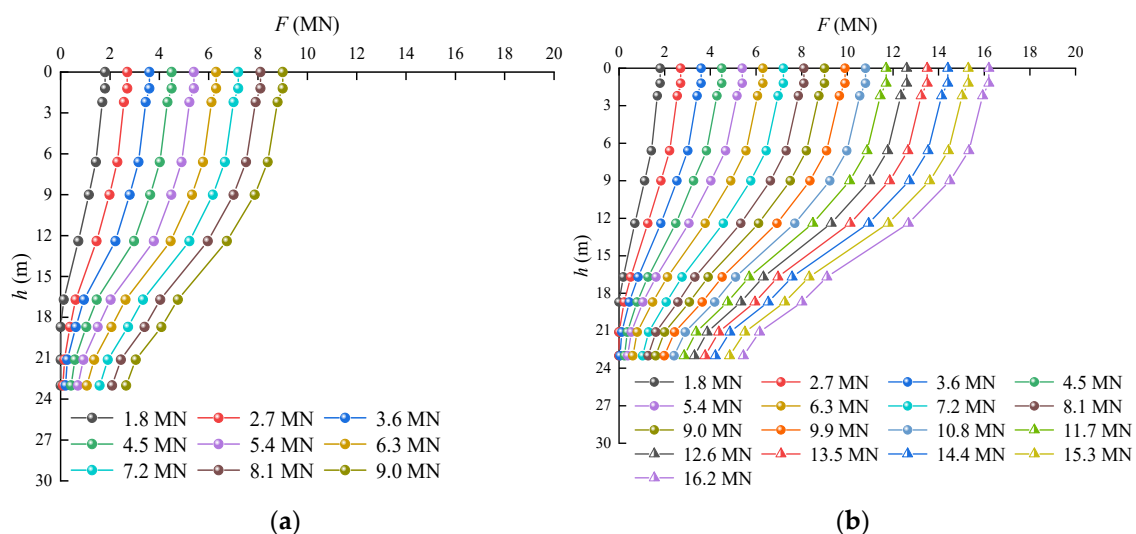
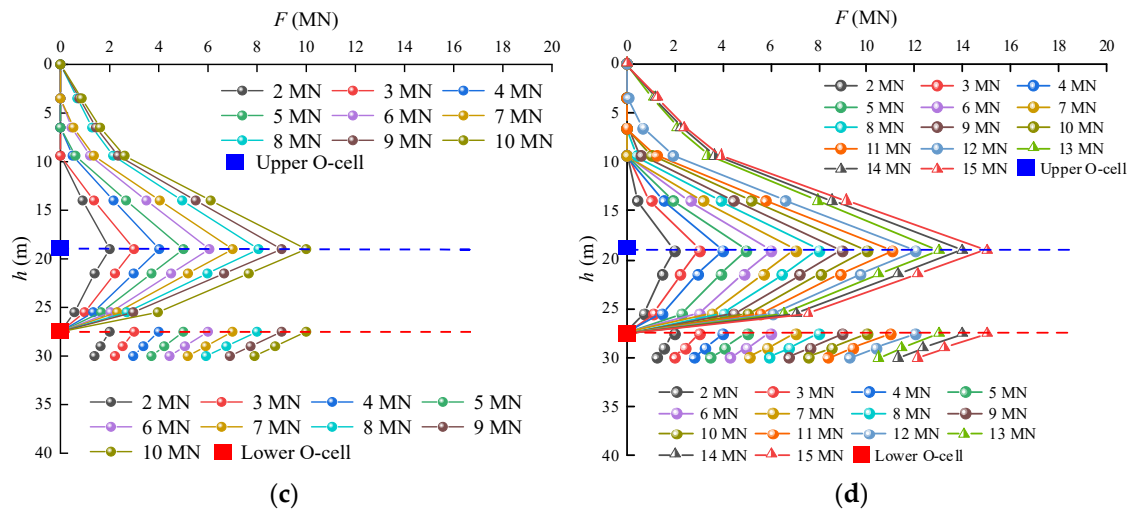


Figure 10. Cont.



**Figure 10.** Axial force distributions at different loading levels: (a) TP1 before combined grouting; (b) TP1 after combined grouting; (c) TP2 before combined grouting; and (d) TP2 after combined grouting.

As illustrated in Figure 10a,b, the test pile TP1, which was evaluated using the traditional top-down load testing method, exhibits a gradual decrease in axial force with increasing depth across different load levels. During the initial loading phase, the axial force curve exhibits a relatively steep slope, indicating that the side resistance is low and the axial force transferred to the lower part of the pile is minimal. As the load increases, the slope of the axial force curve decreases, indicating a gradual development of side resistance. Concurrently, the axial force in the lower section of the pile increases, while the contribution from end resistance begins to take effect. After the grouting process, the rate at which the axial force in the pile diminishes is significantly greater than that observed in the ungrouted pile. This phenomenon can be attributed mainly to the fact that grouting raises the effective horizontal stress in the surrounding soil. This increase in horizontal stress subsequently enhances the soil's shear strength, leading to a greater side resistance that effectively mitigates the transmission of axial force within the pile.

As shown in Figure 10c,d, the distribution of pile shaft axial force with depth obtained from the bi-directional O-cell test exhibits a clear difference compared to the distribution obtained from the traditional top-down load test. The axial force measured by the bi-directional O-cell test method is highest at the location of the O-cell and gradually decreases both upward and downward along the pile shaft, forming a distribution similar to a triangle. This is primarily due to the axial force near the O-cell being mobilized first and then propagating along the pile shaft in both directions. With the increase in load, the side resistance of test pile TP2 is gradually mobilized, leading to a continuous rise in axial force along the length of the pile shaft. A comparison of the axial force distribution above the O-cell before and after grouting reveals that the axial force curve becomes smoother post-grouting. This indicates a more pronounced variation in axial force with depth under the same load conditions. These observations indicate that the side resistance of the grouted pile has been significantly improved. The grout has positively influenced the physical and mechanical properties of the surrounding soil, thereby effectively mitigating the mudskin problem on the pile shaft. Moreover, under ultimate load conditions, a significant increase in axial force at the pile end positions of both test piles is observed after grouting. This suggests that the combined grouting method has effectively stabilized the soil at the pile end, enhancing both its strength and bearing stiffness.

### 3.3. Average Side Resistance of the Pile

The side resistance of large-diameter bored piles is a crucial factor contributing to their overall bearing capacity, and its effectiveness plays a significant role in determining the performance of the pile foundation. The side resistance of each soil layer under varying load conditions can be determined by analyzing the axial force and the cross-sectional dimensions of the pile shaft. [29]. The bi-directional O-cell test method utilizes a distinct loading technique compared to the traditional top-down load test method. In static load tests, the section of the pile below the O-cell experiences positive friction resistance (upward direction), while the section above the O-cell experiences negative friction resistance (downward direction). According to the relevant provisions in JGJ/T 403-2017 [19], the side resistance of the pile above the O-cell is equivalently converted. The distribution curves of the average side resistance ( $q_{si}$ ) along the depth ( $h$ ) for test piles TP1 and TP2 before and after grouting under various load levels are shown in Figure 11.

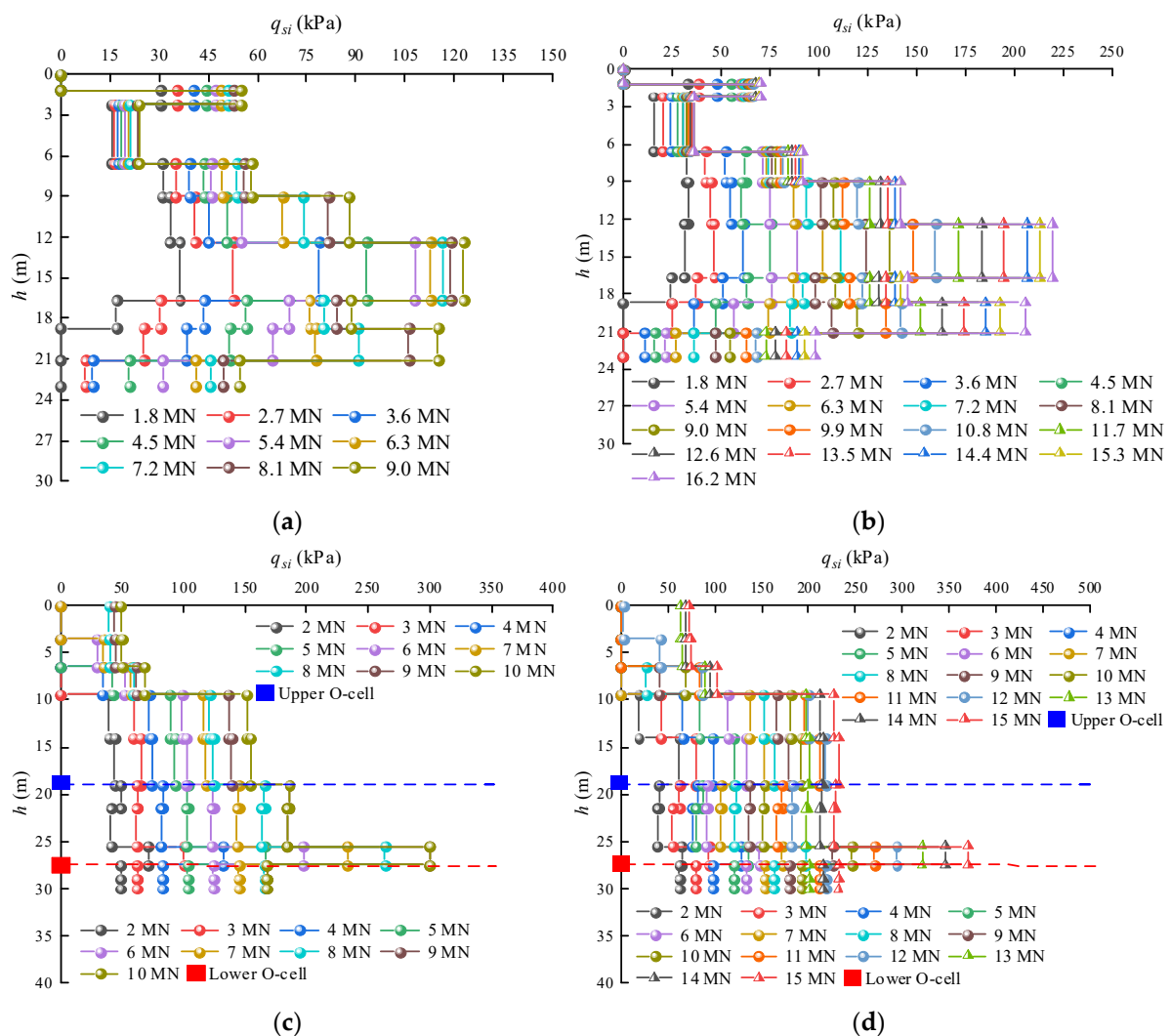


**Figure 11.** Side resistance distributions at different loading levels: (a) TP1 before combined grouting; (b) TP1 after combined grouting; (c) TP2 before combined grouting; and (d) TP2 after combined grouting.

Figure 11 indicates that the distribution of side resistance varies as a result of the differing properties of the soil layers. Even with similar soil properties, side resistance can vary at different depths. In the case of test pile TP1, the side resistance in the upper soil layer manifests before that in the lower soil layer. With the increase in load, the side resistance of the upper soil layer reaches stability more rapidly compared to that of the

lower soil layer. In contrast, for test pile TP2, the side resistance near the O-cell is more fully mobilized. Under identical loading conditions, the side resistance in the lower section of the pile typically exceeds that of the upper section. This phenomenon can be explained by the differences in loading methods between the bi-directional O-cell test and the traditional top-down load test. Therefore, the mobilization of side resistance is not only influenced by the properties of the soil layers and the burial depth but is also closely related to the location of the applied load.

Figure 12 illustrates the distribution curves of the measured side resistance as a function of depth for two test piles subjected to ultimate loading conditions. Figure 11 shows that the side resistance at various depths after grouting surpasses the levels observed before grouting, with maximum increases of 81.03% and 50.01%, respectively. Additionally, the ultimate side resistance values measured using the bi-directional O-cell test method for the two test piles at the same soil layer can be compared to the ultimate side resistance values measured using the top-down load test method. The specific formula is shown below. This comparison allows for the further calculation of the self-balancing conversion coefficients for each soil layer before and after grouting, as shown in Table 3.

$$\gamma_i = q_{si} / q_{si}' \quad (1)$$

where  $i$  is the number of soil layers;  $q_{si}$  is the side resistance of the ( $i$ )-th layer of soil measured by the bi-directional O-cell test method; and  $q_{si}'$  is the side resistance of the ( $i$ )-th layer of soil measured by the top-down load test method.

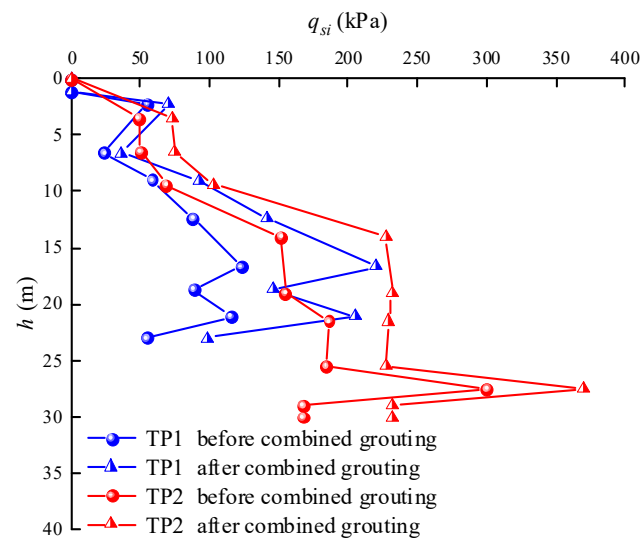


**Figure 12.** Distribution of side resistance of test piles at different depths under ultimate load conditions.

**Table 3.** Comparison of the side resistance and  $\gamma$  values of each soil layer before and after combined grouting.

Soil Layer	Ultimate Side Resistance (kPa)					
	Bi-Directional O-Cell Test Method		Top-Down Load Test Method		$\gamma$	
	Before Grouting	After Grouting	Before Grouting	After Grouting	Before Grouting	After Grouting
Silty sand	49.9	74.80	58.25	92.00	0.86	0.81
Gravel	306.13	459.21	380.73	669.47	0.80	0.69

Table 3 shows that the side resistance conversion factors for the silty sand layer before and after grouting are 0.86 and 0.81, while those for the gravel layer are 0.80 and 0.69, respectively. This indicates that the cement grout injected during the post-grouting process

effectively addressed certain defects between the pile shaft and the borehole wall, resulting in a robust bond between the grout, the pile shaft, and the surrounding soil. As a result, the load-bearing capacity of the pile side was notably enhanced, which in turn led to a considerable increase in the side resistance.

### 3.4. End Resistance of the Pile

Figure 12 illustrates the curves of end resistance ( $q_b$ ) versus end displacement ( $s_b$ ) for test piles TP1 and TP2 before and after grouting. Figure 13 demonstrates that, during the initial loading phase, there is a rapid increase in end resistance as end displacement rises. As the load continues to increase, the end resistance exhibits a gradual rise. With the ultimate load, the end resistance of TP1 after grouting is 5.45 MN, which is a 105.66% increase compared to the tip resistance of 2.65 MN before grouting. For TP2, the end resistance after grouting is 12.09 MN, a 53.04% increase from the tip resistance of 7.90 MN before grouting. This indicates that the combined grouting technique is effective in improving the end settlement issue in bored piles. Furthermore, the response speed of end resistance after grouting is faster for each test pile. For example, after grouting in TP2, when the end displacement reaches 1.73 mm, the corresponding end resistance is already close to 5.92 MN, which is similar to the pre-grouting value, while the corresponding end displacement before grouting is 3.94 mm. The end displacement after grouting is only 43.91% of the pre-grouting value, indicating that the grouted bored pile has significantly stronger resistance to settlement and deformation. The pressurized grout effectively strengthens the soil layer and sediment at the pile end through mechanisms such as permeation, compaction, and fracturing, thereby significantly enhancing the strength and stiffness of the soil layer at the pile end.

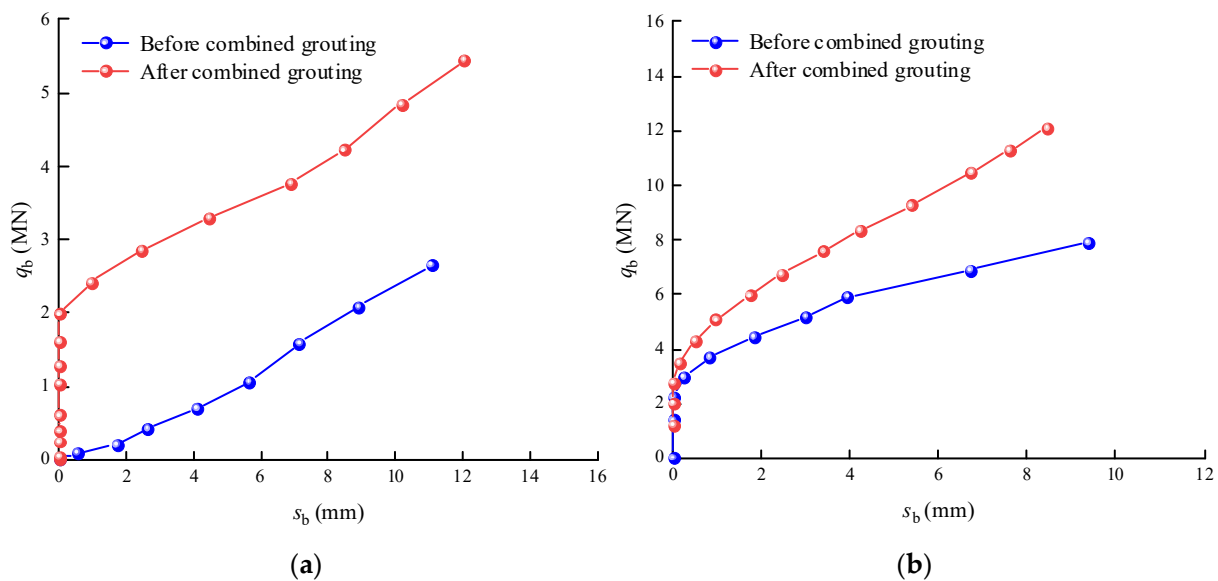


Figure 13. End resistance versus end displacement curves of the test piles: (a) TP1 and (b) TP2.

## 4. Comparison of Methods for Calculating the Characteristic Values of End-Bearing Capacity

### 4.1. Calculation Results Using the Standard Method

According to Equation 6.3.4 in the “JTG3363-2019 Specifications for the design of foundations of highway bridges and culverts” [30], the characteristic value of end-bearing capacity,  $q_b$ , for bored piles is calculated as follows:

$$q_b = m_0 \lambda [f_{a0} + k_2 \gamma_2 (h - 3)] \quad (2)$$

where  $q_b$  is the modified characteristic value of the end-bearing capacity;  $m_0$  is the bottom cleaning coefficient;  $\lambda$  is the correction coefficient;  $f_{a0}$  is the characteristic value of the initial end-bearing capacity;  $k_2$  is the depth correction coefficient for the bearing capacity characteristic value;  $\gamma_2$  is the weighted average unit weight of the soil layers above the pile end; and  $h$  is the embedment depth of the pile end.

Based on the geological parameters of each soil layer shown in Table 1, the corresponding values are obtained according to the specification [30], as presented in Table 4. According to Equation (2), the end-bearing capacity characteristic value for TP1 is 1261.26 kPa. For TP2, it is 1681.80 kPa.

**Table 4.** Standard empirical parameter values.

Test Pile No.	Soil Layer at the Pile End	$m_0$	$\lambda$	$f_{a0}$ (kPa)	$k_2$	$\gamma_2$ (kN/m <sup>3</sup> )	$h$ (m)	$q_b$ (kPa)
TP1	Gravel	0.7	0.7	550	5.0	20.24	23	1261.26
TP2	Gravel	0.7	0.7	550	5.0	21.35	30	1681.80

#### 4.2. Comparison of Field Test Results Using the Bi-Directional O-Cell Test and Top-Down Load Test Methods

The measured end-bearing capacities of test pile TP1 tested using the top-down load test method and test pile TP2 tested using the bi-directional O-cell test method, divided by the corresponding pile end areas for each pile, can provide the characteristic values of the actual end-bearing capacity for each test pile. The specific formula is as follows:

$$q_b = Q_p / A_p \quad (3)$$

where  $Q_p$  is the pile end resistance and  $A_p$  is the cross-sectional area of the pile end.

The field parameters for test piles TP1 and TP2 are shown in Table 5. According to Equation (3), the characteristic value of the end soil bearing capacity for TP1 is calculated as 2347.84 kPa, and it is calculated as 3929.14 kPa for TP2.

**Table 5.** Field test parameters of each test pile.

Test Pile No.	Soil Layer at the Pile End	$A_p$ (m <sup>2</sup> )	$Q_p$ (kN)	$q_b$ (kPa)
TP1	Gravel	1.1304	2654	2347.84
TP2	Gravel	2.0096	7896	3929.14

#### 4.3. Comparison and Analysis of Calculation Results

The comparison of the end-bearing capacity characteristic value measured by the bi-directional O-cell test method, the top-down load test method, and the code method is shown in Figure 13. As shown in Figure 14, the end-bearing capacity characteristic values obtained from the bi-directional O-cell test and top-down load test methods in the field tests are significantly higher than those calculated using the current code formulas. Specifically, the end-bearing capacity measured by the bi-directional O-cell test method is 133.63% higher than the value calculated by the code method, while the top-down load test method yields a value 86.15% higher than the code-calculated value. Compared to the field test results, the calculated values using the current code formulas are relatively conservative and clearly underestimate the actual end-bearing capacity in engineering practice, which results in the design of excessively long piles for highway bridges. The comparison of the bi-directional O-cell test method and top-down load test method shows that the bi-directional O-cell test method takes full advantage of the O-cell placed near the

pile end, enabling direct and accurate measurement of the end bearing capacity, thereby maximizing the ultimate bearing capacity of the soil at the pile end. In contrast to the traditional top-down load test method, the bi-directional O-cell test method provides a faster and more accurate evaluation of the end-bearing capacity, benefiting both designers and construction personnel.

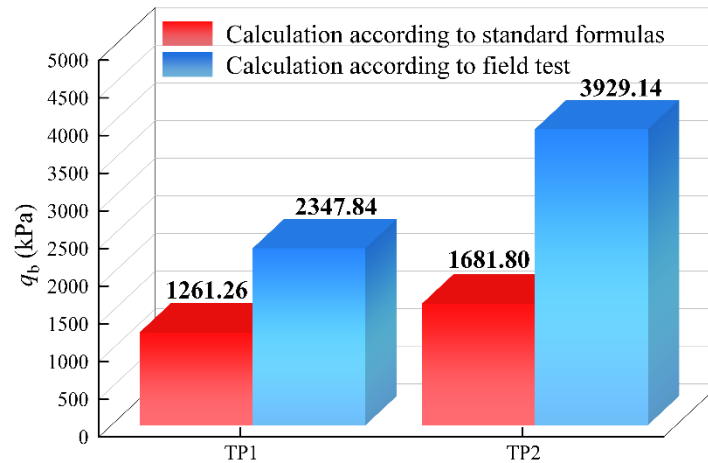


**Figure 14.** Comparison of characteristic values of end-bearing capacity obtained from various static load test methods.

## 5. Conclusions

This paper is based on two large-diameter cast-in-place piles from the Wushi to Yiyang Expressway project and investigates the vertical bearing capacity, deformation characteristics, and load transfer patterns of the composite grouting piles before and after grouting using the bi-directional O-cell and top-down load testing methods. It also examines the values of the conversion coefficient  $\gamma$  for different soil layers used in the bi-directional O-cell test method for calculating bearing capacity. The characteristic values of the pile end soil-bearing capacity obtained from bi-directional O-cell tests and top-down load tests are compared with the values calculated using formulas from current standards, verifying the accuracy of the existing standards and traditional static loading methods. The following conclusions are drawn:

1. The stress distribution along the pile shaft differs significantly between the bi-directional O-cell test method and the top-down load test method. In the bi-directional O-cell test, the side resistance develops from the end to the top, whereas in the top-down load test, the side resistance develops from the top towards the end.
2. Combined grouting enables the cement grout to fill, compact, and split into various soil layers, which improves the physical and mechanical properties of the soil layers around the piles and fully enhances the mechanical characteristics of the pile–soil interface. Meanwhile, it plays a solidifying role in the soil at the pile end, enhancing the strength and stiffness of the soil at that location. The maximum increases in the side and end resistance of the pile are 81.03% and 105.35%, respectively.
3. The side resistance conversion coefficients for the silty sand layer and gravel layer before and after grouting are 0.86 and 0.80 and 0.81 and 0.69, respectively. This indicates that the cement grout has eliminated some defects between the pile shaft and the borehole wall, forming a strong bond between the grout, the pile shaft, and the surrounding soil. Consequently, the load-bearing characteristics of the pile side were significantly improved, leading to a substantial increase in the side resistance. The research results can provide a valuable reference for similar projects.

4. The characteristic values of the end-bearing capacity measured by the bi-directional O-cell test method and the load test method in field tests are 133.63% and 86.15% higher, respectively, than the calculated values based on the current highway bridge and culvert specifications. Both the current specification formulas and the measured values of the load test method are overly conservative, underestimating the pile end-bearing capacity in practical engineering. It is recommended that future designs combine bi-directional O-cell testing with composite grouting techniques to further optimize pile foundation design.

**Author Contributions:** Conceptualization, Y.D. and K.Q.; methodology, R.-Z.Z.; software, R.-Z.Z.; formal analysis, Y.D. and K.Q.; investigation, Y.D. and R.-Z.Z.; resources, F.Z. and Z.-H.W.; data curation, Z.-H.W.; writing-original draft preparation, Y.D. and K.Q.; writing-review and editing, Z.-H.W. and F.Z.; visualization, Y.D.; supervision, Z.-H.W. and F.Z. All authors have read and agreed to the published version of the manuscript.

**Funding:** This work was supported by the National Natural Science Foundation of China (52008100), the Natural Science Foundation of Jiangsu Province (BK20200400), the China Postdoctoral Science Foundation(2022M723534), the Natural Science Foundation of Jiangsu Higher Education Institutions of China (23KJA560005), and the Special Foundation for Technology Innovation of Carbon Peak and Carbon Neutral in Jiangsu Province (BE2022605).

**Data Availability Statement:** The data are available upon reasonable request.

**Conflicts of Interest:** Author Yu Du was employed by the Comprehensive Urban Management Enforcement Bureau of Yueyang City. The remaining authors declare that they have no known competing financial interests or personal relationships that could have appeared to influence the work reported in this paper.

## References

1. Zhang, Z.M. *Post-Grouting Technology of Bored Piles and Engineering Application*; China Architecture & Building Press: Beijing, China. (In Chinese)
2. Wan, Z.H.; Dai, G.L.; Gong, W.M. Field and theoretical analysis of response of axially loaded grouted drilled shafts in extra-thick fine sand. *Can. Geotech. J.* **2020**, *57*, 391–407. [[CrossRef](#)]
3. Bruce, D.A. Enhancing the performance of large diameter piles by grouting. *Ground Eng.* **1986**, *19*, 9–15.
4. Dai, G.L.; Gong, W.M.; Zhao, X.Q.; Zhao, X.L. Static testing of pile-base post-grouting piles of the suramadu bridge. *Geotech. Test. J.* **2010**, *34*, 34–49. [[CrossRef](#)]
5. Mcvay, M.; Bloomquist, D.; Thiyyakkandii, S.; Lai, P. Experimental study, numerical modeling of and axial prediction approach to base grouted drilled shafts in cohesionless soils. *Acta Geotech.* **2014**, *9*, 439–454.
6. Wan, Z.H.; Dai, G.L.; Gong, W.M. Field study on post-grouting effects of cast-in-place bored piles in extra-thick fine sand layer. *Acta Geotech.* **2019**, *14*, 1357–1377. [[CrossRef](#)]
7. Salem, T.N.; El-Basset, O.H.A.; Hassan, R. 3D Numerical Analysis of Post-Grouted Piles. *Indian Geotech. J.* **2023**, *54*, 1562–1583. [[CrossRef](#)]
8. Mullins, G.; Winters, D.; Steven, D. Predicting end bearing capacity of post-grouted drilled shaft in cohesionless soils. *J. Geotech. Geoenviron. Eng.* **2006**, *132*, 478–487. [[CrossRef](#)]
9. Li, Y.H.; Zhu, X.; Zhou, T.H. Experimental study of effects of pile tip post grouting on bearing characteristics of large-diameter bored pile. *Rock Soil Mech.* **2016**, *37*, 388–396.
10. Zhang, J.Q.; Zhao, C.F.; Zhao, G.; Wu, Y.; Gong, X. Pile tip grouting diffusion height prediction considering unloading effect based on cavity reverse expansion model. *Geomech. Eng.* **2024**, *37*, 97–107.
11. Li, J.H.; Wu, Y.P.; Wu, C.H.; Zhu, F.P.; Zhao, Q.W.; Zhang, G.P.; Yan, Z.H.; Xu, R.Q. Study on the diffusion law of grouting slurry at the pile end of bored piles in gravel pebble layers. *Buildings* **2024**, *14*, 2555.
12. Song, M.J.; Song, Y.H.; Jung, M.; Park, Y.H.; Park, J.H.; Lee, J.H.; Chung, M. A Comparison Study between Top-down Load Test and Bi-directional Load Test Analysis Method in Rock-socketed Small Size Drilled Shaft. *J. Korean Geoenviron. Soc.* **2013**, *14*, 5–12.
13. Niazi, F.S.; Wanggensten, Y.; Karl, E. Stacked pile solution for axial load–settlement analysis of driven piles in multi-layered soils. *Can. Geotech. J.* **2020**, *57*, 851–870. [[CrossRef](#)]



14. Zhang, L.; Wang, T.H.; Zhao, Z.K.; Jin, X. Research on bearing difference between single-pile combined foundation field test and group-pile combined foundation of high-rise buildings. *Buildings* **2023**, *13*, 2127.
15. Zhang, J.J.; Gu, X.W.; Ren, G.F.; Zhou, C.E.; Wang, N.X. Centrifugal model tests on deformation characteristics of pile-net composite foundation under super-large loads. *Chin. J. Geotech. Eng.* **2024**, *46*, 212–216. (In Chinese)
16. Osterberg, J. *New Device for Load Testing Driven Piles and Drilled Shaft Separates Friction and End Bearing*; Piling and Deep Foundations; A.A. Balkema: Rotterdam, The Netherlands, 1989; pp. 421–427.
17. Gong, W.M.; Dai, G.L.; Zhang, H.W. Experimental study on pile-end post-grouting piles for superlarge bridge pile foundations. *Front. Struct. Civ. Eng.* **2009**, *3*, 228–233. [[CrossRef](#)]
18. Wang, W.D.; Wang, M.; Wu, J.B. Field study on the ultimate bearing capacity of enlarged grout base of pre-bored grouted planted pile. *Rock Soil Mech.* **2023**, *44*, 3091–3098.
19. *JGJ/T 403-2017*; Technical Specification for Static Loading Test of Self-balanced Method of Building Foundation Piles. China Architecture Publishing & Media Co., Ltd.: Beijing, China, 2017.
20. Dai, G.L.; Gong, W.M.; Cheng, Y.; Xue, G.Y. Application of self-balanced testing and post grouting to large diameter and super-long piles. *Chin. J. Geotech. Eng.* **2005**, *27*, 690–694.
21. Safaqah, O.; Bittner, R.; Zhang, X.G. Post-grouting of drilled shaft tips on the Sutong Bridge: A case study. In Proceedings of the Geo-Denver 2007 Congress: Contemporary Issues in Deep Foundation, Denver, CO, USA, 18–21 February 2007.
22. Nguyen, M.H.; Fellenius, B.H. Bidirectional-cell tests on two 70 m long bored piles in Vietnam. In Proceedings of the GeoInstitute Geo Congress, Geotechnical Special Publication, Reston, VA, USA, 23–26 February 2014; pp. 482–496.
23. Zhou, X.; Wang, C.C.; Liu, X.H.; Xu, X. Research on load bearing performance of post-grouting bored piles in deep and thick pebble layer. *Bridge Constr.* **2023**, *53*, 31–37.
24. Wan, Z.H.; Duan, C.; Hu, T.; Zhou, F.; Dai, G.L. Field study on bearing capacity of large-diameter rock-socketed bored piles with combined grouting in highly weathered rock layers. *Rock Mech. Rock Eng.* **2024**, *57*, 8701–8722. [[CrossRef](#)]
25. *T/CECS G: D67-01-2018*; Technical Specification for Post-grouting of Cast-in-Place Pile of Highway Bridges. China Communications Press: Beijing, China, 2018.
26. Wan, Z.H.; Dai, G.L.; Gong, W.M.; Chen, H.J.; Chen, X.Y. Analysis on the load transfer function of post-grouting bored pile based on self-balanced method. *China Civ. Eng. J.* **2017**, *50*, 98–104. (In Chinese)
27. *JTG/T 3650-2020*; Technical Specifications for Construction of Highway Bridges and Culverts. China Communications Press: Beijing, China, 2020.
28. *JGJ 106-2014*; Technical Code for Testing of Building Foundation Piles. China Architecture Publishing & Media Co., Ltd.: Beijing, China, 2014.
29. Zhou, Z.J.; Xu, F.; Lei, J.T.; Bai, Y.; Chen, C.R.; Xu, T.Y.; Zhang, Z.P.; Zhu, L.X. Experimental study of the influence of different hole-forming methods on the bearing characteristics of post-grouting pile in Loess Areas. *Transp. Geotech.* **2021**, *27*, 100423. [[CrossRef](#)]
30. *JTG 3363-2019*; Specifications for Design of Foundation of Highway Bridges and Culverts. China Architecture Publishing & Media Co., Ltd.: Beijing, China, 2019.

**Disclaimer/Publisher’s Note:** The statements, opinions and data contained in all publications are solely those of the individual author(s) and contributor(s) and not of MDPI and/or the editor(s). MDPI and/or the editor(s) disclaim responsibility for any injury to people or property resulting from any ideas, methods, instructions or products referred to in the content.